

Modelling and Simulation of Phase Transition in Compressed Liquefied CO₂

Sindre Tosse Per Morten Hansen Knut Vaagsaether

Department of Process, Energy and Environment Technology, University College of Southeast Norway, Norway,
knutv@usn.no

Abstract

A model and solution method for phase transition in compressed liquefied gases is presented. The model is a two-phase 6-equation model with a common flow velocity for the two phases. The numerical method for solving the model is based on the 2. order shock capturing MUSCL-scheme with a HLLC Riemann solver. The van der Waal cubic equation of state is used for closing the set of equations. The phase transition model is based on thermodynamic and mechanical relaxation between the phases. The goal of the work is to present a numerical model capable of resolving the two-phase flow situation in the depressurization of a vessel or pipe containing liquefied CO₂. Simulation of expansion and phase transition in pressurized liquefied CO₂ is presented and compared with experimental data. The simulations are with a one dimensional geometry and the experiments are performed in a narrow tube. Wall effects in the experiments are not captured in the simulations. The wave structure seen in the experiments is reproduced by the simulation although not quantitatively. The simulations show that the fluid is in the metastable region before it undergoes a phase transition. The level of expansion of the metastable liquid shown in the in the simulations is not seen in the experiments.

Keywords: phase transition, liquefied gas, BLEVE, van der Waal, MUSCL

1 Introduction

The focus of this paper is to present a numerical model capable of resolving the two-phase flow situation in the depressurization of a vessel or pipe containing liquefied CO₂. The methodology is attended for use with all types of liquefied pressurized gases. Sublimation of solid particles will not be addressed, since liquid-vapour interaction is the dominant process inside and in the immediate vicinity of the vessel. In order to get the necessary level of accuracy in the thermodynamic calculations, a non-monotonic equation of state is chosen. For CO₂, the most accurate liquid-vapour EOS available is the Span-Wagner multiparameter EOS (Span and Wagner, 1996). It would be extremely challenging to implement this type of EOS into a numerical code, but the authors regards this as the end-goal of the present work. The usage of a non-monotonic EOS in a numerical solver raises a number of

issues, since both the liquid and vapour states have a limited region of existence. In order to deal with these issues, the simplest form of a non-monotonic EOS, namely the cubic van der Waals EOS, is used in the development of a numerical code. Menikoff and Plohr (1989) state that the Maxwell equal-area rule must be applied to modify the equation of state in order to avoid imaginary speed of sound in the van der Waals loop. Saurel et al. (2008) propagate the misconception that the square speed of sound is negative in the spinodal zone. In the present work however, a less strict method is applied to allow metastable states, while maintaining a real speed of sound. While quantitatively inaccurate, the van der Waals equation of state provides a qualitative representation of every major feature of real gas behavior. Combined with its simple formulation, this makes it an often used EOS in model development and academic work. Using a non-monotonic equation of state in a numerical solver raises a number of issues. It is therefore necessary to develop robust solving algorithms that are capable of handling two phase flow in the vicinity of spinodal states. The van der Waals EOS is chosen to develop a proof of concept, because its simple formulation allows for analytical expressions for many thermodynamic parameters, e.g. the spinodal curve. Most compressible two-phase solvers use some form of stiffened gas equation of state or a more generalized Mie-Gruneisen form equation of state. Even though it can be written on Mie-Gruneisen form, the van der Waals equation of state has been little used in the context of fluid dynamics. Slemrod (1984) analyzed the dynamic phase transitions in a van der Waals fluid. Zheng et al. (2011) used an interface capturing method with a generalized equation of state on the Mie-Gruneisen form where, among others, the van der Waals equation of state was used. To the authors knowledge, no solvers allowing metastable two-phase compressible flow with phase transition using the van der Waals equation of state exists.

Some work has been done to develop numerical models that are capable of describing evaporation waves. Saurel et al. (1999) developed a Godunov method for compressible multiphase flow that was later applied to the subject of phase transition in metastable liquids (Saurel et al., 2008). They were able to qualitatively reproduce the evaporation front velocities measured by Simoes-Moreira and Shepherd (1999). In recent years, there have been several at-

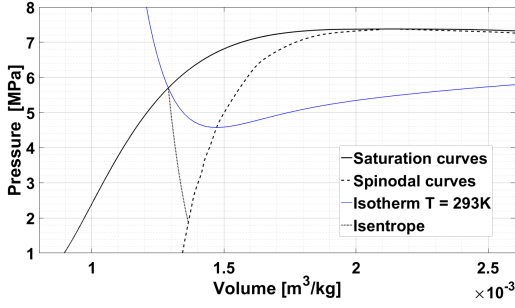


Figure 1. Pressure-volume diagram for CO₂ showing saturation curve, spinodal curve, an isotherm and an isentrope.

tempts to model BLEVE-type scenarios (Pinhasi et al., 2007; VanDerVoort et al., 2012; Xie, 2013).

1.1 Metastable liquids

Figure 1 shows the pressure-volume diagram of CO₂ calculated from the Span-Wagner EOS. The spinodal curve is defined as $\left(\frac{\partial p}{\partial v}\right)_T = 0$ and is seen as an absolute boundary for an expanding liquid state. In the region between the liquid saturation curve and the spinodal curve a metastable liquid can exist. A metastable liquid is not in an equilibrium condition and a fluid can only stay in such a state for very short times. During a rapid expansion of a compressed liquefied gas metastable liquid states will occur behind propagating expansion waves before phase transition forces the thermodynamic state to change towards equilibrium conditions.

2 Model for two phase flow and phase transition

The numerical model used in this work solves the two-pressure 6-equation model given by Saurel et al. (2009). Without heat and mass transfer, the model reads:

$$\frac{\partial \alpha_1}{\partial t} + u \frac{\partial \alpha_1}{\partial x} = \mu(p_1 - p_2), \quad (1)$$

$$\frac{\partial \alpha_1 \rho_1}{\partial t} + \frac{\partial \alpha_1 \rho_1 u}{\partial x} = 0, \quad (2)$$

$$\frac{\partial \alpha_2 \rho_2}{\partial t} + \frac{\partial \alpha_2 \rho_2 u}{\partial x} = 0, \quad (3)$$

$$\frac{\partial \rho u}{\partial t} + \frac{\partial \rho u^2 + (\alpha_1 p_1 + \alpha_2 p_2)}{\partial x} = 0, \quad (4)$$

$$\frac{\partial \alpha_1 \rho_1 e_1}{\partial t} + \frac{\partial \alpha_1 \rho_1 e_1 u}{\partial x} + \alpha_1 p_1 \frac{\partial u}{\partial x} = -p_I \mu(p_1 - p_2), \quad (5)$$

$$\frac{\partial \alpha_2 \rho_2 e_2}{\partial t} + \frac{\partial \alpha_2 \rho_2 e_2 u}{\partial x} + \alpha_2 p_2 \frac{\partial u}{\partial x} = p_I \mu(p_1 - p_2). \quad (6)$$

The right hand side terms corresponds to pressure relaxation. p_I is the interfacial pressure, estimated by

$$p_I = \frac{Z_2 p_1 + Z_1 p_2}{Z_1 + Z_2}, \quad (7)$$

where $Z_k = \rho_k c_k$ is the acoustic impedance of phase k . Where α_k is the volume fraction of phase k , ρ_k is the density of phase k , p_k is the pressure of phase k , e_k is the specific internal energy of phase k , Y_k is the mass fraction of phase k , c_k is the speed of sound of phase k , μ is the dynamic compaction viscosity and determines the rate of pressure relaxation, u is the flow velocity and an infinitesimal relaxation time, or large enough drag, is assumed leading to a common velocity between the phases. Phase 1 and phase 2 is vapour and liquid respectively. The mixture speed of sound used in this model is the frozen speed of sound,

$$c_f^2 = Y_1 c_1^2 + Y_2 c_2^2. \quad (8)$$

In the present work, we use stiff pressure relaxation ($\mu \rightarrow \infty$). As shown in (Saurel et al., 2009), this means the recovery of the 5-equation model. Then the model is strictly hyperbolic with wave speeds $(u + c_f, u - c_f, u)$.

2.1 The van der Waals equation of state

The van der Waals equation of state (vdW-EOS) is the simplest form of a cubic equation of state. It is classified as cubic because it can be written on the form

$$v^3 + a_2 v^2 + a_1 v + a_0 = 0 \quad (9)$$

where v is the specific volume and a_k are pressure and/or temperature dependent coefficients. The vdW-EOS can be derived from the ideal gas EOS by adding correction terms for the excluded volume occupied by finite-sized particles and inter-molecular forces. On its classical form, the vdW-EOS reads

$$\left(p + \frac{n^2 a}{V^2}\right)(V - nb) = n R_M T \quad (10)$$

where n is the number of moles occupying the volume V at pressure p and temperature T . R_M is the ideal gas constant. a is a measure of the attraction between particles and b is the volume excluded by one mole of particles (molecules). As the volume tends to infinity, the vdW-EOS converges to the ideal gas law. The special case of $V = nb$ corresponds to a situation where the volume V is completely filled by the particles. At this point, the pressure tends to infinity. This implies that the van der Waals equation of state is only valid for $V > nb$. In terms of the volume at the critical point, this limit can be written as $\frac{v}{v_c} > \frac{1}{3}$.

3 Solver

The equation set is solved by the 2. order accurate shock capturing MUSCL-scheme (Monotone Upstream-centered Scheme for Conservation Laws) combined with a HLLC (Harten Lax vanLeer Contact) Riemann solver for the interfacial fluxes (Toro, 1999). This solver is used for the hyperbolic part of the equation set i.e. the left hand side of equations 2 to 6.

The shock capturing method with the approximate Riemann solver solves shock waves and contact surfaces as very steep gradients with a numerical diffusion of a shock or contact discontinuity thickness of usually three control volumes. The equation set is closed by the van der Waals equation of state. The time step is variable and controlled by the Courant-Friedrich-Levy number.

3.1 Stiff pressure relaxation

The pressure relaxation step solves the equation set

$$\frac{\partial \alpha_1}{\partial t} = \mu(p_1 - p_2), \quad (11)$$

$$\frac{\partial \alpha_1 \rho_1 e_1}{\partial t} = -p_1 \mu(p_1 - p_2), \quad (12)$$

$$\frac{\partial \alpha_2 \rho_2 e_2}{\partial t} = p_1 \mu(p_1 - p_2) \quad (13)$$

in the limit $\mu \rightarrow \infty$. All other conserved variable groups are held constant during the relaxation step. According to (Saurel et al., 2009), this system of equations can be replaced by

$$e_k(p, v_k) - e_k^0(p_k^0, v_k^0) + \hat{p}_I(v_k - v_k^0) = 0, \quad k = 1, 2 \quad (14)$$

and the saturation constraint

$$(\alpha \rho)_{1v_1} + (\alpha \rho)_{2v_2} = 1 \quad (15)$$

where $(\alpha \rho)_k$ is constant during the relaxation step. The system can be closed by the van der Waal equation of state $e_k(\rho_k, p_k)$. Equation 14 can then be reformulated to $v_k(p)$ by using an estimate of \hat{p}_I . In the present work, the estimation $\hat{p}_I = p_I^0$ is used, but other estimates can also be used as shown by Saurel et al. (2009). Finally, we insert the expressions for v_k into eq. 15 and solve for p .

Since the pressure estimated by this method is not guaranteed to be in agreement with the mixture equation of state $p(\rho, e, \alpha_1)$, this pressure is only used to find the relaxed volume fraction α_1 . The relaxed pressure is then determined by the mixture equation of state and the internal energy from the redundant total energy equation. The conserved variables $(\alpha \rho e)_k$ are then re-initialized using the relaxed pressure and volume fraction. This ensures the conservation of mixture energy in the flow field.

Alternate relaxation methods can also be used. Both isentropic and isenthalpic relaxation methods has been tested with the same results as the method described here. This gives reason to assume that the thermodynamic relaxation path is of lesser importance, since it is only used to estimate the relaxed volume fraction. If the numerical method is expanded to a more complex EOS, this means that the pressure relaxation process most likely can be resolved with a less rigorous estimate of the thermodynamic relaxation path.

With the reduced vdW-EOS, eq. 14 can be written as

$$\pi(\delta_k) = \frac{2C_k \delta_k^2 \hat{\pi}_I - 2\delta_k^3 \hat{\pi}_I - 3\delta_k + 3}{\delta_k^2 (3\delta_k - 1)}, \quad (16)$$

where

$$C_k = \delta_k^0 + \frac{1}{\hat{\pi}_I} \left[\frac{1}{2} (\pi_k^0 + \frac{3}{(\delta_k^0)^2}) (3\delta_k^0 - 1) - \frac{3}{\delta_k^0} \right]. \quad (17)$$

Since we have no mass transfer, we can write

$$G_1 \delta_1 + G_2 \delta_2 = 1. \quad (18)$$

where $G_k = (\alpha \rho)_{k v_c}$. From this, we get

$$\delta_2(\delta_1) = \frac{1 - G_1 \delta_1}{G_2} \quad (19)$$

The algorithm for stiff pressure relaxation solves the equation $f(\delta_1) = 0$ by the Newton-Raphson method, where

$$f(\delta_1) = \pi_1(\delta_1) - \pi_2(\delta_1),$$

$$\frac{d\pi_k}{d\delta_1} = \left(-\hat{\pi}_I \frac{6C_k - 2}{(3\delta_k - 1)^2} + \frac{6(3\delta_k^2 - 5\delta_k + 1)}{\delta_k^3 (3\delta_k - 1)^2} \right) d_k,$$

$$d_1 = 1, \quad d_2 = -\frac{G_1}{G_2}$$

Where π is reduced pressure and δ is reduced volume.

3.2 Stiff thermodynamic relaxation

The thermodynamic relaxation method used presently differs somewhat from the methods used by Saurel et al. (2008) and Zein et al. (2010). It is simpler in formulation and relatively easy to implement for any equation of state. We consider a two phase system with total density $\rho = \alpha_1 \rho_1 + \alpha_2 \rho_2$ and total internal energy $e = Y_1 e_1 + Y_2 e_2$. Since no mass or heat is added to the system during the relaxation step, these mixture properties are constant. We will consider the velocity of the two phases to be equal and constant during the relaxation step. Initially, the system is closed by the known variables ρ_1, ρ_2, e_1, e_2 . In the numerical solver used presently, the two phases will be in mechanical equilibrium at the start of the relaxation step, but this is not a prerequisite of the procedure. The system can be uniquely determined by requiring complete thermodynamic equilibrium between the two phases:

$$p_1 = p_2 = p, \quad T_1 = T_2 = T, \quad g_1 = g_2 = g. \quad (20)$$

Where g is the Gibbs free energy. Note that this requirement is not possible for all ρ and e . This is indeed the case when there is only a single phase solution, that is when the limit of complete evaporation or condensation is reached. Since the numerical method is only valid for $\alpha_k > \xi$, where ξ is some small number (typically $\xi = 10^{-6}$), the single phase limit of phase 1 will be determined by

$$p_1 = p_2 = p, \quad T_1 = T_2 = T, \quad \alpha_1 = 1 - \xi \quad (21)$$

and equivalent for the single phase limit of phase 2. If a cubic equation of state is used, even this is not possible for all ρ and e . This will be the case when one phase reaches the spinodal state before thermal equilibrium is reached. If

phase 2 is at the spinodal state, the system is determined by

$$\begin{aligned} p_1 = p_2 = p_{\text{spin}}(v_2) = p, \\ T_1 = T(v_1, p), T_2 = T_{\text{spin}}(v_2), \alpha_1 = 1 - \xi \end{aligned} \quad (22)$$

v_2 is determined by the mixture equation of state, and v_1 is determined by conservation of mass ($v = Y_1 v_1 + Y_2 v_2$). The subscript *spin* denotes the thermodynamic spinodal state.

In the context of the van der Waals EOS, the three cases (20, 21 and 22) can be identified by the values of ρ and e . A fourth case is theoretically possible, namely $e < e(\rho)_{T=0}$, but this is not likely to occur in numerical calculations and is therefore not further examined.

The stiff thermodynamic relaxation procedure was used when $p_l < p_{\text{sat}}(T_l)$. An additional criterion $\xi_I < \alpha_1 < 1 - \xi_I$ can be used, where ξ_I represents the interface limit of the volume fraction (typically $\xi_I = 10^2 \xi$ to $10^3 \xi$). This last criterion is referred to as the interface criterion of the thermodynamic relaxation procedure and is used to allow for the formation of metastable liquid.

4 Experiments

The capabilities of the model to predict phase transition in pressurized liquid CO₂ by expansion is validated by comparing simulation results with experimental results. The experimental results are presented in Hansen et al. (2016). Figure 2 shows a drawing of a experimental apparatus for rapid expansion of liquefied CO₂. The expansion tube is 9 mm inner diameter, 1.5 mm wall thickness polycarbonate. Before the beginning of the experiment, the tube is filled to about half level with saturated liquid CO₂ at room temperature, about 20°C. The pressure in the tube is then 5.5 MPa. The top of the tube is closed with a diaphragm which is punctured by an arrow, releasing CO₂ to the atmosphere. Expansion waves then propagates down the tube and starts a boiling process due to the falling pressure. The expansion tube is transparent and a high speed digital camera captures the expansion and boiling process on a high speed movie which is later analyzed. The camera operates at 20 000 fps for this experiment. Typical wave trajectories is shown in figure 3.

5 Simulation set-up

The simulation domain is shown with initial conditions in figure 4. The calculation was run with an initial CFL number set to 0.2 for the first 200 time steps. The CFL number was then linearly increased to 0.5 over 50 time steps and was set to 0.5 for the rest of the calculation. The initial conditions for the simulation is shown in table 1. The one dimensional domain was divided into 7000 control volumes with 10^{-4} m length.

6 Results and discussion

The van der Waal EOS is not able to reproduce the thermodynamical states quantitatively, especially close to satura-

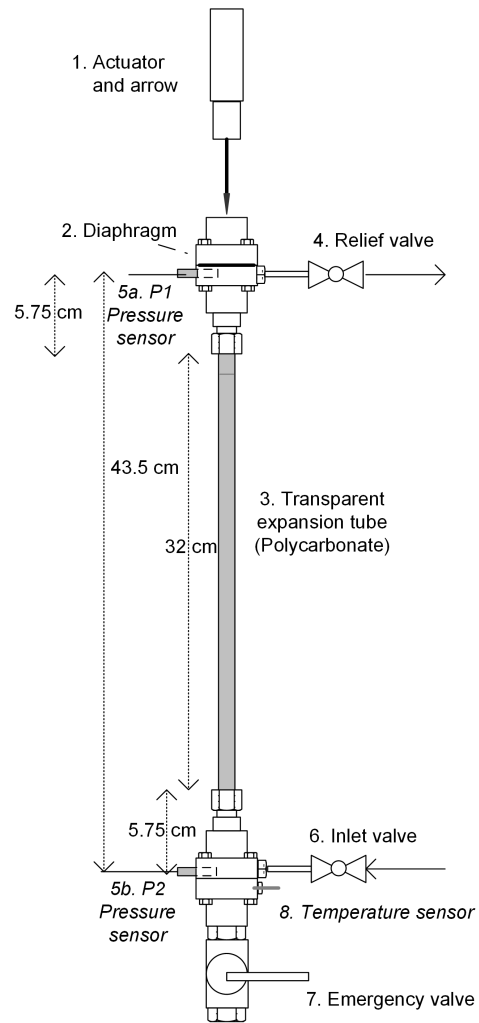


Figure 2. Experimental set-up.

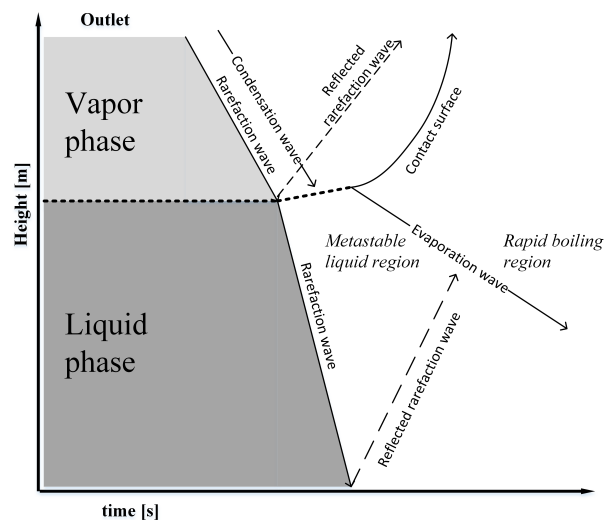


Figure 3. Schematic representation of the waves in the one dimensional expansion experiments.

tion condition. The results are presented as scaled quantities to show the qualitative behaviour of the simulation method. The pressure is scaled with saturation pressure

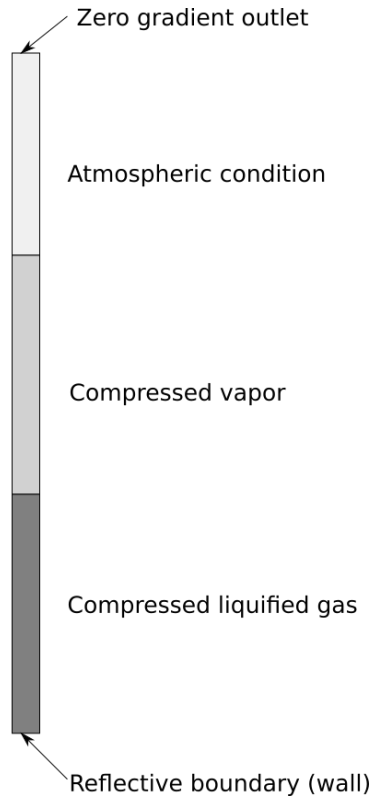


Figure 4. Initial and boundary conditions in the simulation domain.

Table 1. INITIAL SIMULATION CONDITIONS

	$x < 0.25\text{ m}$	$0.25\text{ m} \geq x < 0.5\text{ m}$	$x \geq 0.5\text{ m}$
p [Pa]	$5.5 \cdot 10^6$	$5.5 \cdot 10^6$	10^5
u [m/s]	0	0	0
α	10^{-6}	$1 - 10^{-6}$	$1 - 10^{-6}$
ρ_1 [kg/m ³]	175.00	175.00	1.8794
ρ_2 [kg/m ³]	530.45	565.46	565.46

at initial temperature, ie. the initial pressure in the tube. The time is scaled by the average propagation time for an expansion wave along the total length of the pipe and the position is scaled by the tube length. The initial interphase in the experiments was 56 % of the tube length from the bottom. For comparison of the wave structures the interphase is moved to scaled position 0.5 like in the simulations. The wave structures in the experiments and simulations are shown as x-t diagrams. The experimental x-t diagram is extracted from the high speed movie. The pixel row from the central position of the tube is stacked along the time vector.

Figure 5 shows the simulated wave structure in the expansion tube. An initial expansion wave propagates downwards in the gas phase from scaled time 0. The expansion wave both reflects and transmits at the interphase, at scaled time 0.7, where the reflected wave is seen traveling upwards and the transmitted wave continues down-

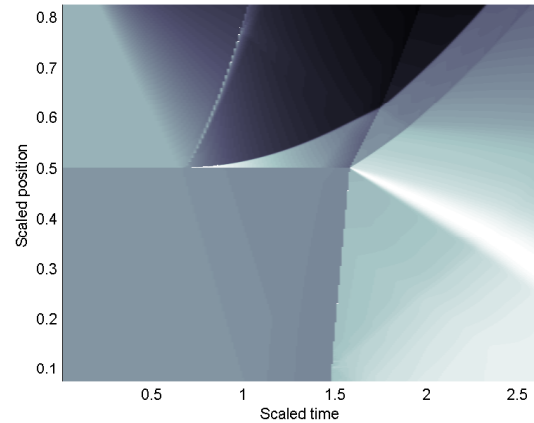


Figure 5. Scaled simulated density for expansion of CO₂ in 1D-domain. The results show the wave structure in the expansion process.

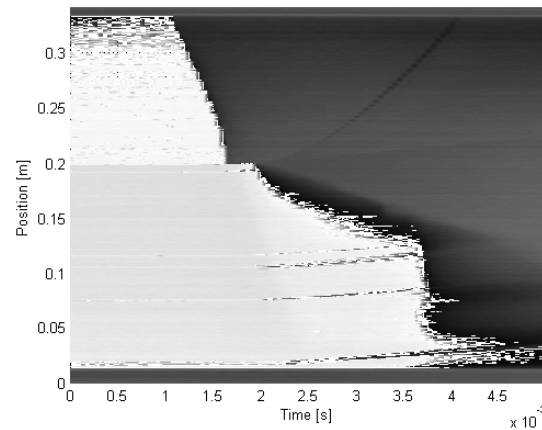


Figure 6. Experimental x-t diagram of expansion of CO₂ in a narrow tube. The results show the wave structure in the expansion process.

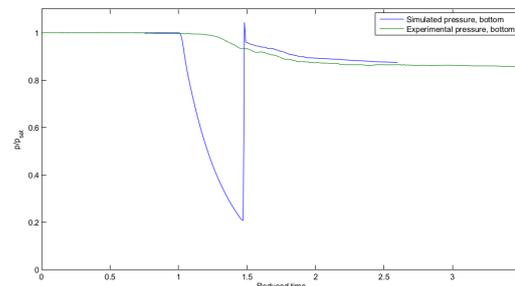


Figure 7. Simulated and experimental scaled pressure history at the bottom of the expansion tube.

wards into the liquid. A condensation phase transition occurs behind the reflected upwards traveling expansion wave. A phase transition in the liquid is initiated and the contact surface of the expanding liquid-gas mixture travels upwards following the reflected expansion wave. The

expansion wave traveling through the liquid is reflected at the bottom of the tube and a faster phase transition is initiated there due to the high level of expansion. The phase transition initiated by the incident expansion wave is slow due to a low level of superheat. Once the expansion wave reflects at the bottom and again interacts with the initial interphase between liquid and vapour, at scaled time 1.6, a faster phase transition is triggered. Comparing these results to the experimental results seen in figure 6 shows the same wave structures. In the experiments a condensation wave following the incident expansion wave occurs. This is not seen in the simulations. The reflected expansion wave is not clearly seen in the experimental x-t diagram. The condensation seen in the simulations will not occur in experiments since the wave propagates into a two phase fluid.

Figure 7 shows the relative scaled pressure at the bottom of the tube vs. scaled time for simulation and experiment. The large drop in the simulated pressure, not seen in the experiments, is due to the expanding liquid. The thermodynamical state in the expansion wave is highly expanded metastable liquid. When the liquid pressure reaches the spinodal state at scaled time 1.5, a very rapid phase transition occurs and brings the pressure up towards equilibrium pressure. This creates a shock wave propagating upwards due to the fast expansion in the boiling. This shock is driven by a sudden change in thermodynamic state to equilibrium. This rapid phase transition propagates with the mesh speed, ie. $\Delta x/\Delta t$ and is an artefact of the phase transition model. The experimental pressure values does not drop as dramatically as the simulated pressure. The reason for this discrepancy can be that nucleation sites along the narrow tube will force a faster phase transition in the metastable liquid and keep the pressure at a higher level. The wall effects are not included in the simulation. After the rapid phase transition and formation of the shock wave the simulated pressure is close to the experimental pressure.

7 Conclusions

A model and solver for rapid phase transition in compressed liquefied gases is presented. The phase transition model uses a mechanical and thermodynamical relaxation approach for phase transition. The present model and solver is capable of handling the wave types that can occur in a depressurization process however the combination of the van der Waals equation of state and an ideal geometry in one dimension will not produce the quantitative values seen in the experiments. Wall effects and low accuracy of the EOS close to saturation conditions and in metastable state causes a higher degree of superheat before a rapid phase transition can occur in the simulations. When the metastable liquid reaches the spinodal state, the model produces an unphysically fast evaporation wave. Future work to improve the simulation method will be to develop a kinetic based phase transition model in highly expanded

metastable liquids. Such a model can reduce the possibility of low pressures seen in the metastable liquid during the reflection of rarefaction waves. A kinetic based transition rate can include wall effects and effects from impurities in the liquid. For higher accuracy the present method can be extended to more complex equations of states, like the Span-Wagner EOS.

References

- P. M. Hansen, K. Vaagsaether, A. V. Gaathaug and D. Bjerketvedt. CO₂ explosions - an experimental study of rapid phase transition. *8th International Seminar on Fire and Explosion Hazards*, 25. – 28. April, Hefei, China, 2016.
- R. Menikoff and B.J. Plohr. The Riemann Problem for Fluid-Flow of Real Materials. *Reviews of Modern Physics*, 61(1):75–130, 1989.
- G. A. Pinhasi, A. Ullmann, and A. Dayan. 1D plane numerical model for boiling liquid expanding vapor explosion (BLEVE). *International Journal of Heat and Mass Transfer*, 50(23-24):4780–4795, 2007.
- R. Saurel, and R. Abgrall. A multiphase Godunov method for compressible multifluid and multiphase flows. *Journal of Computational Physics*, 150(2):425–467, 1999.
- R. Saurel, F. Petitpas, and R. Abgrall. Modelling phase transition in metastable liquids: application to cavitating and flashing flows. *Journal of Fluid Mechanics*, 607:313–350, 2008.
- R. Saurel, F. Petitpas, and R. A. Berry. Simple and efficient relaxation methods for interfaces separating compressible fluids, cavitating flows and shocks in multiphase mixtures. *Journal of Computational Physics*, 228(5):1678–1712, 2009.
- J.R. Simoes-Moreira and J.E. Shepherd. Evaporation waves in superheated dodecane. *Journal of Fluid Mechanics*, 382:63–86, 1999.
- M. Slemrod. Dynamic phase transitions in a van der Waals fluid. *Journal of Differential Equations*, 52(1):1–23, 1984.
- R. Span and W. Wagner. A new equation of state for carbon dioxide covering the fluid region from the triple-point temperature to 1100 K at pressures up to 800 MPa. *Journal of Physical and Chemical Reference Data*, 25(6):1509–1596, 1996.
- E. F. Toro. *Riemann solvers and numerical methods for fluid dynamics*. Springer-Verlag, Heidelberg, second edition, 1999.
- M. M. Voort, A. C. Berg, D. J. E. M. Roekaerts, M. Xie, and P. C. J. Bruijn. Blast from explosive evaporation

of carbon dioxide: experiment, modeling and physics. *Shock Waves*, 22(2):129–140, 2012.

M. Xie. "*Thermodynamic and Gasdynamic Aspects of a Boiling Liquid Expanding Vapour Explosion.*" *PhD thesis, Delft University of Technology*, 2013.

A. Zein, M. Hantke, and G. Warnecke. Modeling phase transition for compressible two-phase flows applied to metastable liquids. *Journal of Computational Physics*, 229(8):2964–2998, 2010.

H. W. Zheng, C. Shu, Y. T. Chew, and N. Qin. A solution adaptive simulation of compressible multi-fluid flows with general equation of state. *International Journal for Numerical Methods in Fluids*, 67(5):616–637, 2011.